IEEE Photonics Journal
An IEEE Photonics Society Publication

Dual-View Integral Imaging System With Wide Viewing Angle And High Spatial Resolution

Volume 12, Number 3, June 2020

Huan Deng
Sai Li
Lei Wang
Yan Xing
Qiong-Hua Wang

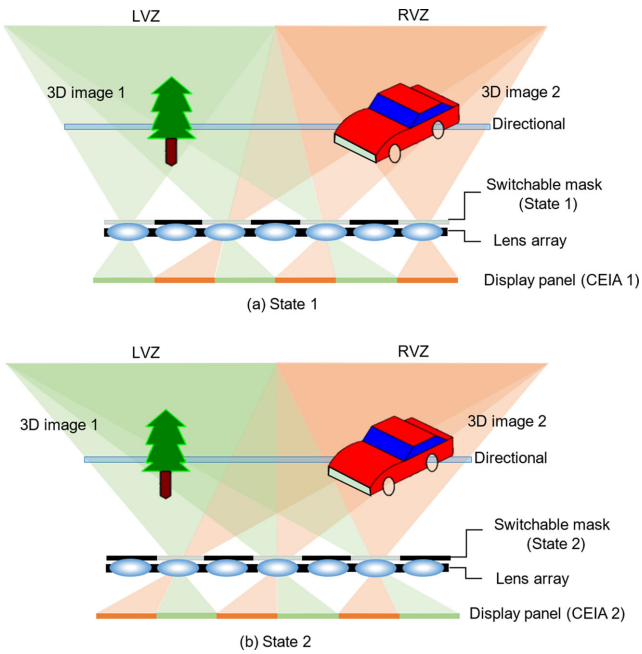

DOI: 10.1109/JPHOT.2020.2994118

Dual-View Integral Imaging System With Wide Viewing Angle And High Spatial Resolution

Huan Deng,[1] **Sai Li**,[1] **Lei Wang**,[1] **Yan Xing**,[2] **and Qiong-Hua Wang** [2]

[1]School of Electronics and Information Engineering, Sichuan University, Chengdu 610065, China
[2]School of Instrumentation and Optoelectronic Engineering, Beihang University, Beijing 100191, China

DOI:10.1109/JPHOT.2020.2994118

Manuscript received March 19, 2020; revised May 4, 2020; accepted May 8, 2020. Date of publication May 11, 2020; date of current version May 26, 2020. This work was supported in part by the National Natural Science Foundation of China under Grant 61775151, and in part by the Innovative Spark Project of Sichuan University under Grant 2018SCUH0003. Corresponding author: Qiong-Hua Wang (e-mail: qionghua@buaa.edu.cn).

Abstract: In this paper, a dual-view integral imaging system is proposed to present two different 3D images for viewers in different viewing zones. For most of the conventional dual-view integral imaging systems, either the viewing angle or the spatial resolution of 3D image is decreased. In the proposed dual-view system, the viewing angle of each viewing zone is enlarged by introducing a switchable mask. Meanwhile, the spatial resolution of the 3D image is maintained by using the time-division multiplexing technology. A prototype of the proposed dual-view system is developed and it has wide viewing angle and high spatial resolution. The experiments coincide with the theoretical analysis.

Index Terms: Dual-view, integral imaging, viewing angle, spatial resolution.

1. Introduction

Dual-View display is a new type of display technology appeared in recent years [1]–[3]. It displays two different images on one screen simultaneously, and provides multiple viewers in different viewing directions with different images so that the viewers can observe their desired image from one screen at the same time [4]–[6]. For instance, in the vehicle display system, the dual-view display allows the driver on the left side watch the navigation information, and the passengers on the right side watch the movies. In surgical operation scenarios, doctors can see the patient's status information during the operation, and assistants can check other information meanwhile. On the other hand, three-dimensional (3D) display which includes holographic display [7]–[10], volumetric display [11], super multi-view display [12], light field display [13], [14], and integral imaging [15]–[17] brings a vivid visual experience to the audiences, and has become an important part of the display technologies. Integral imaging, as one of the most promising 3D display technologies, has the advantages of full and smooth parallax, and visual fatigue free [18]–[21]. Therefore, the combination of the dual-view display and II has attracted increasing attentions from researchers [22]–[30].

Many research groups have devoted to the research of this combination. A dual-view integral imaging system divides the image elements of elemental image array (EIA) into two sub-image elements, and reconstructs different 3D images on the left and right sides, respectively [26].

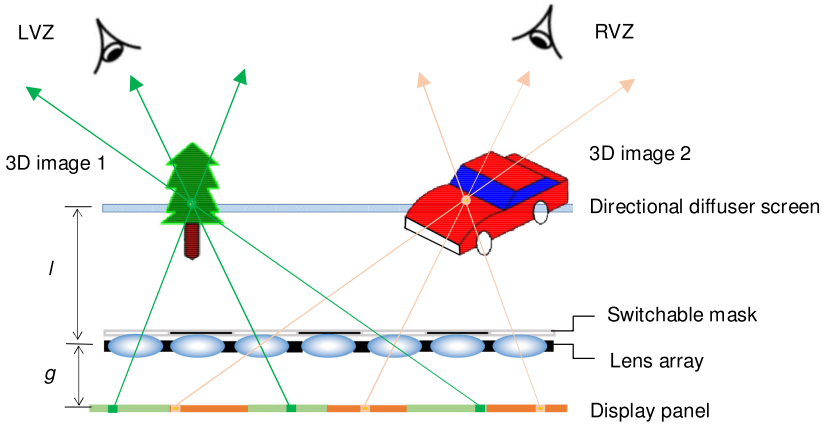

Fig. 1. Schematic diagram of the proposed dual-view integral imaging system.

However, the viewing angle of this system is decreased to half of the conventional mono-view integral imaging system. Another dual-view integral imaging system using a polarization parallax barrier was proposed to increase the viewing angle [27], but the spatial resolution of the 3D image is reduced to half of the mono-view integral imaging system. A dual-view II display using an orthogonal polarizer array and a polarization switcher effectively improves the resolution of 3D image [28], but the viewing angle is still not good. Recently, a dual-view II system used polarized glasses has been proposed. The viewing angle of the system is not limited by the optimal viewing distance [29], but there is still a problem of decreased resolution. In our former work, we propose a dual-view II 3D display system based on a large-pitch lens array and a directional diffuser screen [30], [31]. Although the large-pitch lens array and the directional diffuser screen greatly improve the display performance of the system, it still has the problems of small viewing angle.

In this paper, we propose a dual-view integral imaging system with a wide viewing angle by using an electrically controlled switchable mask. By using the time-division multiplexing technology, the system also can obtain the spatial resolution as high as the conventional mono-view integral imaging system.

2. Principle

2.1 Structure of the Proposed Dual-View Integral Imaging System

The structure of the proposed dual-view integral imaging system is shown in Fig. 1. It mainly consists of a 2D display panel, a lens array, a switchable mask, and a directional diffuser screen. Two compound elemental image arrays (CEIA) are shown on the 2D display alternately, and each CEIA composes of different perspectives of two different 3D scenes. Light rays emitted from the CEIA are modulated by the lens array, and the elemental images (EI) of the CEIA are imaged onto the central depth plane (CDP) through the lens array. The depth of the CDP l is determined by the Gaussian imaging law, which is $\frac{1}{l} + \frac{1}{g} = \frac{1}{f}$, where g is the gap between lens array and the 2D display panel, and f is the focal length of the lens array. The switchable mask is basically a chessboard-patterned mask which is electrically controlled to switch between two patterns. The switchable mask is used to block the light rays passing through certain lenses of the lens array, and it can be attached to any of the two sides of the lens array. In the proposed dual-view integral imaging system shown in Fig. 1, the switchable mask is attached in front of the lens array. The directional diffuser screen located on the CDP receives the images of the EIs and diffuses the lights of each pixel to make the discrete light field of the reconstructed 3D image continuous. The proposed system can reconstruct different 3D images in left viewing zone (LVZ) and right viewing zone (RVZ) with wide viewing angle and high spatial resolution.

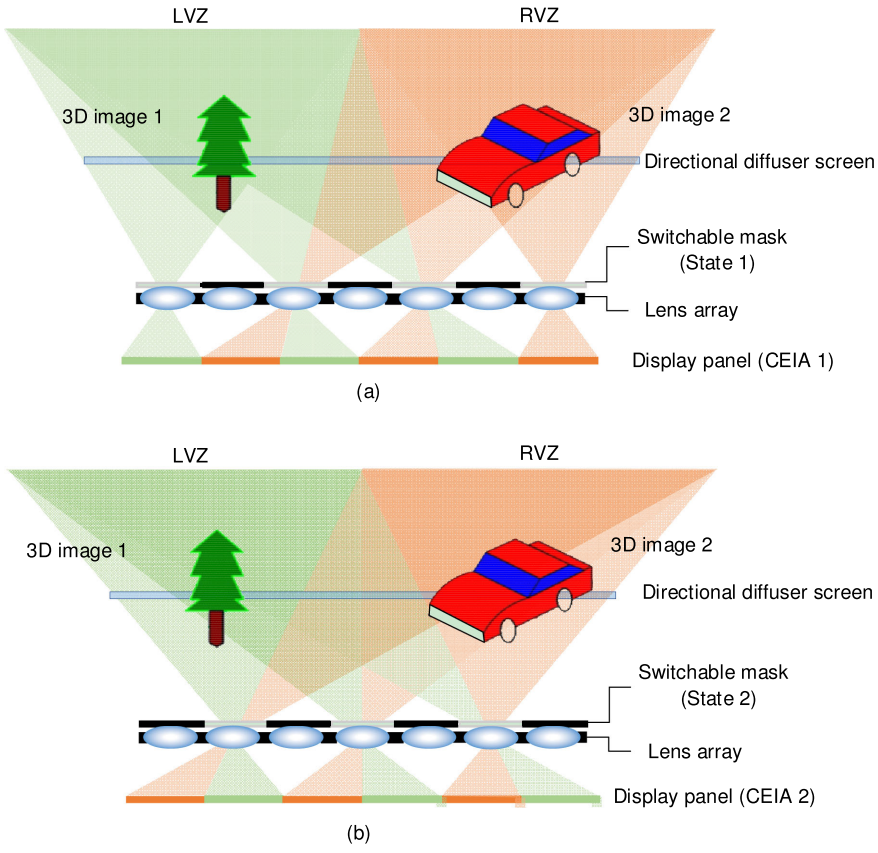

Fig. 2. Principle of the proposed dual-view integral imaging system. (a) State 1 and (b) State 2.

2.2 Operation Principle of The Proposed Dual-View Integral Imaging System

The operation principle of the proposed dual-view integral imaging system is shown in Fig. 2. Unlike the conventional mono-view integral imaging system in which each lens images for only one EI, in the proposed dual-view system, each lens images for two EIs. As shown in Fig. 2, light rays from the green EIs are modulated by the lens array and form the LVZ. Likewise, light rays from the orange EIs form the RVZ. In this case, the lens requires only half as many elements as the EIs. To achieve this requirement, the switchable mask is used to block the light passing through the adjacent lenses so that only half of the lenses in the lens array can work normally. In the proposed dual-view integral imaging system, each of the two viewing zones, LVZ and RVZ, is approximately as wide as the conventional mono-view integral imaging system, so our proposed system can obtain a wide viewing angle. The viewer in the LVZ can only observe the 3D image 1 which is formed by half EIs of the CEIA, and the viewer in the RVZ can only observe the 3D image 2 which is formed by the other half. To achieve as high resolution of 3D image as the conventional mono-view integral imaging system, the proposed dual-view integral imaging system works in two states alternately, as shown in Figs. 2(a) and (b). The 2D display panel shows CEIA 1 in state 1 and CEIA 2 in state 2, respectively, and the switchable mask appears as pattern 1 in state 1 and pattern 2 in state 2, respectively.

The chessboard-patterned switchable mask consists of black and white squared grids, and the side length of each grid is the same as the pitch of the lens array. Light rays arrived at the switchable mask are blocked by the black grids and pass through the white grids. As mentioned above, the switchable mask appears two different patterns in different states of the proposed system. The two

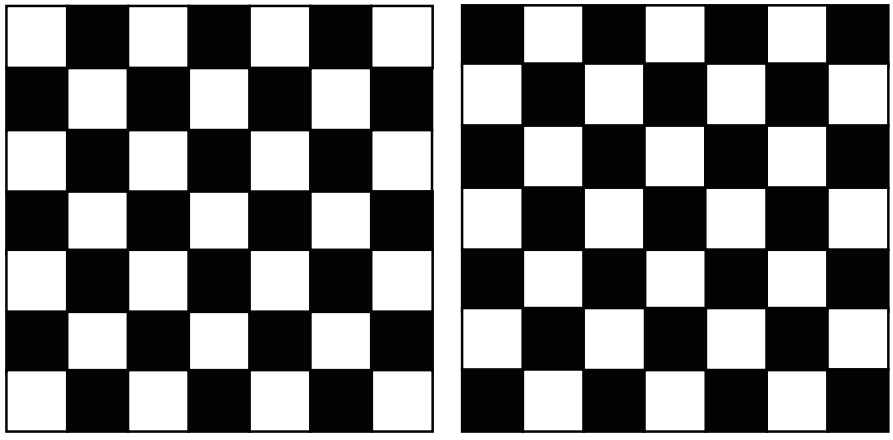

(a) (b)

Fig. 3. Chessboard-patterns appeared on the switchable mask. (a) Pattern 1 and (b) Pattern 2.

patterns are black and white complementary at the same grids, as shown in Fig. 3. $M_1(i, j)$ and $M_2(i, j)$ denote the light transmittance of the ith row and jth column grid of the switchable mask when it appears as pattern 1 and pattern 2, respectively. They can be expressed as Eqs. (1) and (2). A simple way to realize the function of switchable mask is to display the chessboard patterns on a liquid crystal panel, and alternately switch the two different patterns between state 1 and state 2.

$$M_1(i, j) = \begin{cases} 1, & \text{for } i + j \text{ is even} \\ 0, & \text{else} \end{cases} \tag{1}$$

$$M_2(i, j) = \begin{cases} 1, & \text{for } i + j \text{ is odd} \\ 0, & \text{else} \end{cases} \tag{2}$$

In the proposed dual-view integral imaging system, the CEIA contains a set of EIs captured from two 3D scenes. As shown in Fig. 4, the generation process of CEIA can be divided into two steps. Firstly, the LEIA and REIA are generated from left 3D scene 1 and right 3D scene 2 respectively. Then, LEIA and REIA perform Boolean logic operation with the switchable mask, and the operation can be expressed as:

$$\mathrm{CEIA}_1(i, j) = \mathrm{LEIA}(i, j)\,\&\,\mathrm{M}_1(i, j) || \mathrm{REIA}(i, j)\,\&\,!\,\mathrm{M}_1(i, j) \tag{3}$$

$$\mathrm{CEIA}_2(i, j) = \mathrm{LEIA}(i, j)\,\&\,\mathrm{M}_2(i, j) || \mathrm{REIA}(i, j)\,\&\,!\mathrm{M}_2(i, j) \tag{4}$$

where symbol & denotes Boolean AND operation, symbol || denotes Boolean OR operation, symbol ! denotes Boolean NOT operation, and (i, j) denotes the ith row and jth column EI or grid. By the cooperative working of the CEIA and the switchable mask, light rays from the EIs of two different 3D scenes are modulated by the lens array and reconstruct two separate 3D images in the space, so that viewers in different viewing zones can observe different 3D images. The display panel presents CEIA 1 and CEIA 2 alternately and the switchable mask switches synchronously. When the refresh rate is high enough, viewers can obtain 3D images with high spatial resolution, due to persistence of vision.

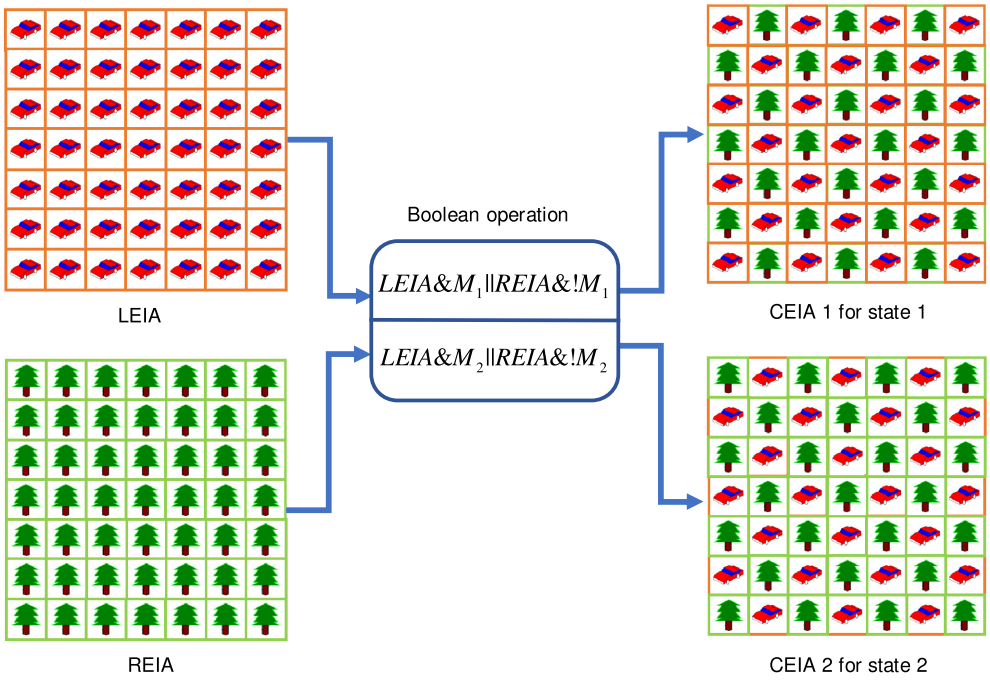

Fig. 4. Generation of CEIA.

2.3 Display Performance of the Proposed Dual-View Integral Imaging System

The viewing angle, spatial resolution and depth of field are three important technical indicators being used to evaluate the display performances of a 3D display system. For most of the dual-view integral imaging systems, either the viewing angle or the spatial resolution of 3D image is decreased to achieve dual-view function, thus the viewing comfortableness is affected. While in the proposed dual-view integral imaging system, both the viewing angle and spatial resolution are enhanced to be approximately as same as that of the conventional mono-view integral imaging system.

In the conventional mono-view integral imaging system, the pitch of the lens equals to the size of EI, so that each lens covers an EI. As shown in Fig. 5(a), the viewing angle of each imaging unit, composed of a lens and an EI, is paralleled to each other, thus the public viewing angle of the system is very small. The viewing angle of this system can be expressed as [32]

$$\theta_c = 2\arctan\left[\frac{p}{2g} - \frac{p(N-1)}{2L}\right] \tag{5}$$

where p is the pitch of the lens array,g is the gap between the lens array and the display panel, N is the amount of lens in one dimension, and L is the viewing distance. In our previous work, we proposed a toed-in structure, as shown in Fig. 5(b), to enlarge the viewing angle of the conventional mono-view system by setting a little larger pitch of the EI than that of the lens. The viewing angle of the toed-in structural system can be expressed as [30], [32]

$$\theta = 2\arctan\left[\frac{p'}{2g}\right] = 2\arctan\left[\frac{p}{2g} + \frac{p}{2L}\right] \tag{6}$$

where p' is the size of the enlarged EI. By this way, the viewing angle of this system can break through the constraint of the lens amount and reaches a level as large as the viewing angle of every single imaging unit of the parallel system. However, seeing from Eq. (6), the larger p' is, the larger θ is. So, the viewing angle is still limited by the size of EI.

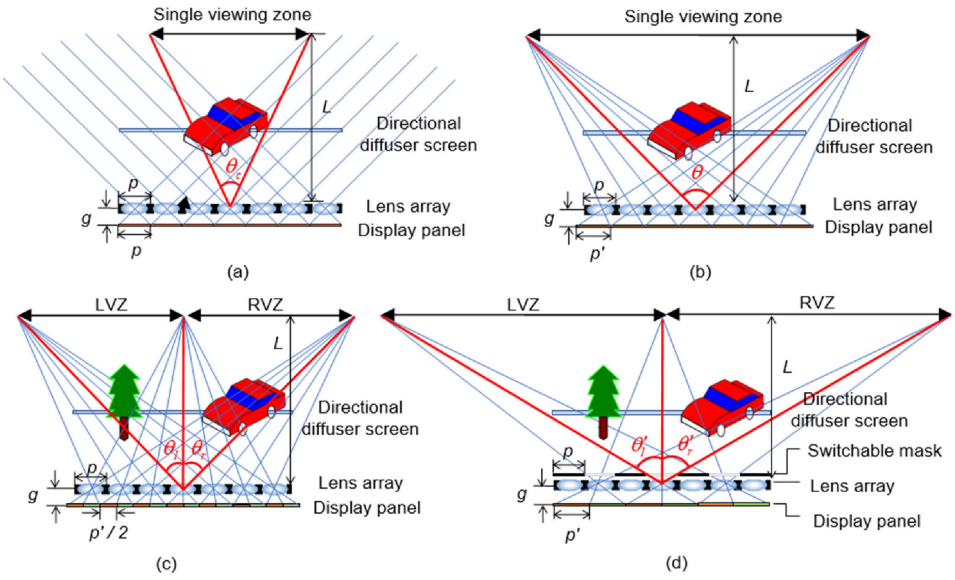

Fig. 5. Viewing angles of different system structures. (a) conventional mono-view integral imaging system in which the size of the EI equals the pitch of the lens, (b) mono-view integral imaging system in which the pitch of the EI is a little larger than that of the lens, (c) former dual-view integral imaging system in Ref [30] in which each EI is divided into left EI and right EI, and (d) the proposed dual-view integral imaging system in which half of the lens are shielded and the sizes of both left and right EIs are enlarged.

When we applied the toed-in structure to the former dual-view integral imaging system, as shown in Fig. 5(c), each EI is divided into two parts which are the left EI and right EI, so the LVZ and RVZ share the viewing angle of the system [30]. As a result, the viewing angle of each viewing zone is reduced to be as half as mono-view integral imaging system.

$$\theta_l = \theta_r = \frac{\theta}{2} = \arctan\left[\frac{p}{2g} + \frac{p}{2L}\right] \tag{7}$$

where θ_l and θ_r are the viewing angles of the LVZ and RVZ of the former dual-view integral imaging system.

To enlarge the viewing angles of LVZ and RVZ, in our currently proposed dual-view integral imaging system we introduce a chessboard-patterned mask to block half of the lens, so that each of the remaining lens covers two EIs, and meanwhile we enlarge both left EI and right EI to have as large size as the EIs of mono-view integral imaging system. Therefore the viewing angles of LVZ and RVZ are both approximately equal to that of the mono-view integral imaging system in Eq. (6).

$$\theta_l' = \theta_r' = \arctan\left[\frac{p'}{g}\right] = \arctan\left[\frac{p}{g} + \frac{p}{L}\right] \tag{8}$$

where θ_l' and θ_r' are the viewing angles of the LVZ and RVZ of the proposed dual-view integral imaging system. By this way, the viewing angle of the proposed dual-view integral imaging system is greatly larger than the former dual-view integral imaging system.

In the integral imaging system, viewers can see partial pixels of each EI through the lens array and form 3D perception with all these pixels, so the spatial resolution of 3D image is the pixel quantity which composes the image. The spatial resolution is mainly determined by the pixel density of the EI and the lens amount. To improve the spatial resolution of 3D image, we could, on one hand, adopt a display panel with higher pixel density, or on the other hand, increase the quantity of lenses. In the proposed system, because of the blocking effect of the switchable mask, only half of

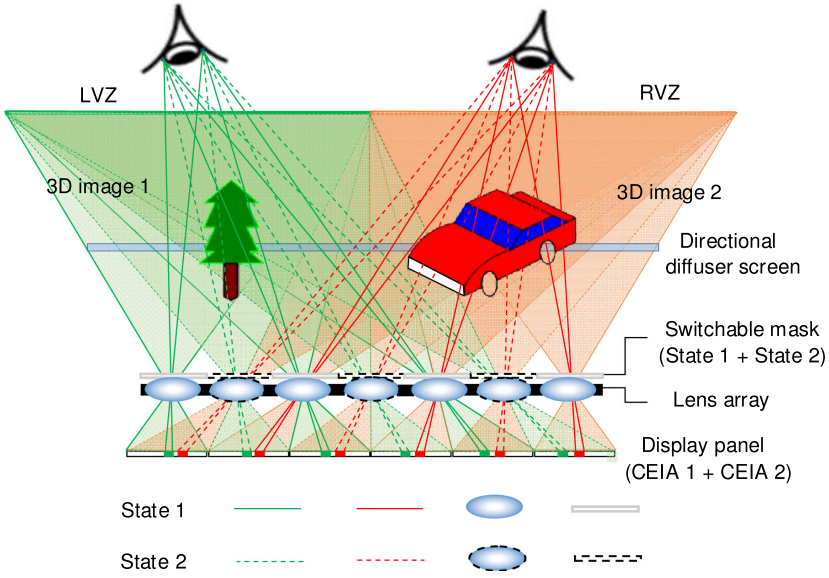

Fig. 6. 3D reconstruction when the system switches between State 1 and State 2 within the visual retention time.

the lenses work normally in each state. So, the switchable mask has to be switched between two states to make the viewer observe the 3D images reconstructed by all the lenses at different time slot. Fig. 6 shows the principle of this method, where the solid lines denote the 3D reconstruction process in state 1, and the dash lines denote the 3D reconstruction process in state 2. In this system, the display panel presents CEIA 1 and CEIA 2 in state 1 and state 2, respectively, and the switchable mask switches synchronously.

For the viewer in the LVZ, he or she can see portions of EIs through half lenses of the lens array in state 1 and portions of EIs through the rest half lenses of the lens array in state 2, as the green solid and dash lines show. So, the viewer in the LVZ observes two 3D images of “tree” at different moment, and the two 3D images are spatially interlaced. Likewise, the viewer in the RVZ also can observe two 3D images of “car” at different moment, as the red solid and dash lines show. When the CEIA and the switchable mask are switched fast enough between the two states, both viewers can observe 3D images with high spatial resolution as much as the conventional mono-view integral imaging system.

The depth of field (DOF) of the integral imaging system can be expressed as [30], [33].

$$\mathrm{DOF} = \frac{2l^2 \Delta r}{gp} \tag{9}$$

where l is the gap between lens array and the directional diffuser screen, Δr is the pixel size of the display panel. Eq. (9) indicates that the DOF is irrelevant to neither the quantity of lens nor the size of EIs. So the proposed dual-view integral imaging system has the same DOF as the conventional mono-view and dual-view integral imaging systems.

According to the above analysis, the proposed dual-view integral imaging system can enlarge the viewing angle and maintain the high spatial resolution by using the time-division multiplexing technology.

3. Experiments and Discussions

In the experiment, an experimental prototype is built up, as shown in Fig. 7. A 23.6-inch liquid crystal display (Dell P2415Q) with the resolution of 3840 $\times$ 2160 and the pixel size of 137um is

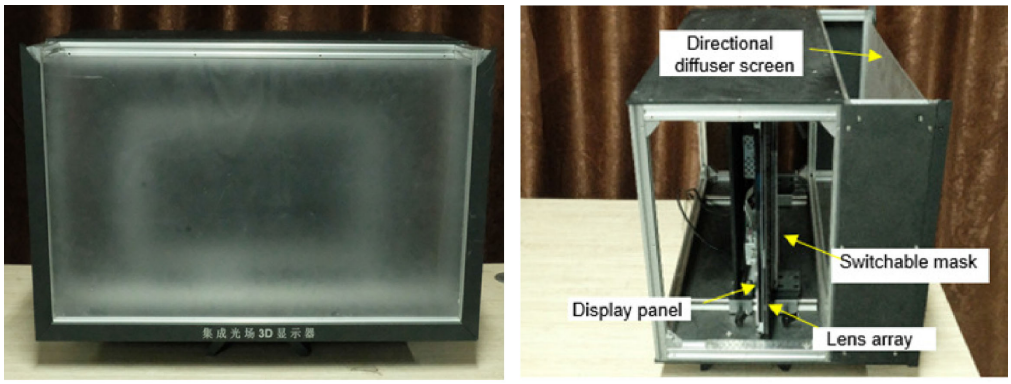

(a) (b)

Fig. 7. Experimental prototype of the proposed dual-view integral imaging system: (a) Front view and (b) Side view.

TABLE 1
Specifications of the Experimental Prototype

Devices	Parameters	Values
Display panel	Product model	Dell P2415Q
	Diagonal Size	23.6 inch
	2D resolution	3840×2160 pixel
	Pixel size Δr	137um
	Size of EI p'	14.8mm
Switchable mask	Product model	BOE06CD
	Diagonal Size	15.6 inch
	2D resolution	3840×2160 pixel
Lens array	Lens number	35×20
	Diameter	12.7mm
	Pitch p	14.7mm
	Focal length f	12.7mm
Directional diffuser screen	Diffusion angle	5°
Others	Distance between display panel and lens array g	13.4mm
	Distance between display panel and directional diffuser screen l	243mm
	Viewing distance L	2000mm

used to display the CEIAs, and the lens array is made by inlaying 35 × 20 plano-convex lenses in a perforated epoxy board. These lenses are in rectangular arrangement with the lens pitch of 14.7 mm and focal length of 12.7 mm. The gap between the display panel and lens array g is set to 13.4 mm which is larger than the focal length of the lens array f, so that the system works on resolution-priority mode. According to the Gaussian imaging law, the CDP of the system is 243 mm away from the lens array. Another liquid crystal panel (BOE06CD) is used to function as the switchable mask whose grid size is the same as that of the EI. The directional diffuser screen (Luminit Company), located on the CDP, has a diffusion angle of 5° × 5°. More detailed specifications of the experimental prototype are shown in Table 1.

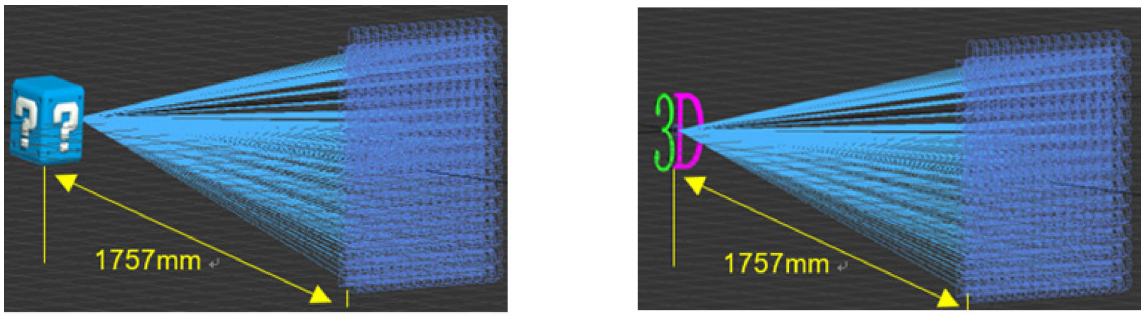

Fig. 8. Virtual 3D scenes and camera array. (a) 3D scene 1, (b) 3D scene 2.

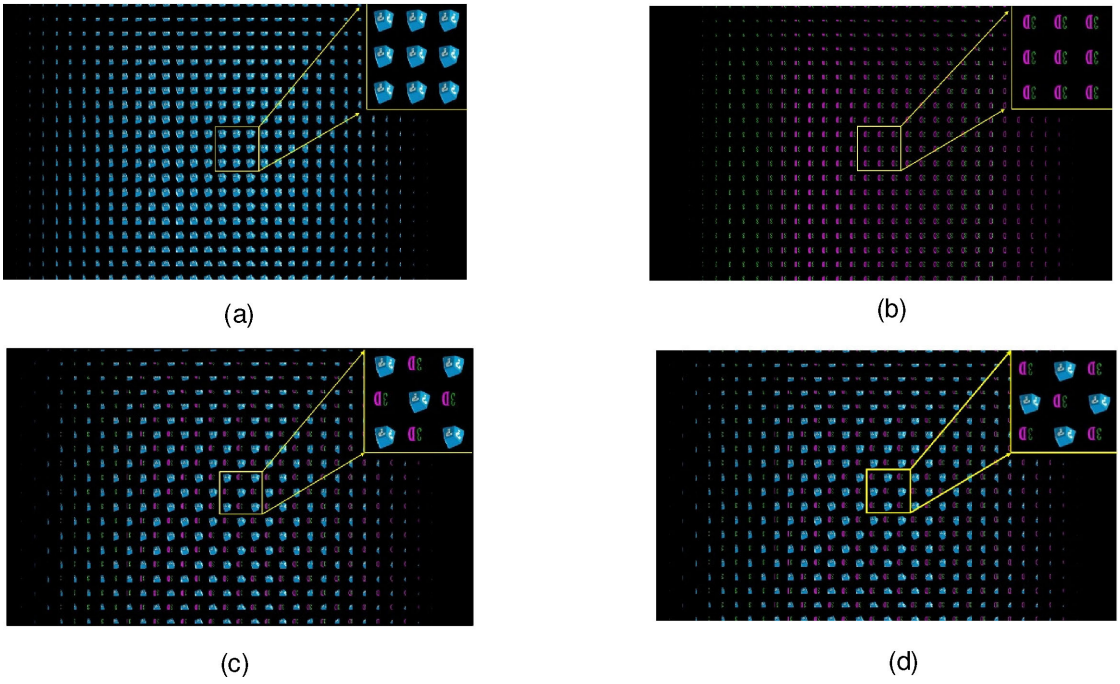

Fig. 9. (a) LEIA of 3D scene 1, (b) REIA of 3D scene 2, (c) CEIA 1, and (d) CEIA 2 for the proposed dual-view integral imaging system.

Two 3D scenes (3D scene 1 “Blue square”, and 3D scene 2 “3D”) were built up by using 3DsMax software in a computer. They were all placed at the distance of 1757 mm from the camera array, as shown in Fig. 8. The size of “blue square” is 13 cm $\times$ 12 cm, and the size of “3D” is 11 cm $\times$ 10 cm. A camera array is set up to capture different perspectives of the two 3D scenes, and then generate the LEIA of 3D scene 1 and REIA of 3D scene 2, as shown in Figs. 9(a) and 9(b), respectively. Boolean logic operation between the LEIA, REIA and switchable mask is carried out, and then we obtain CEIA 1 for state 1 and CEIA 2 for state 2 as shown in Figs. 9(c) and 9(d), respectively.

Fig. 10 shows the dual-view 3D display effect of our proposed system shoot at different viewing positions. As shown in Figs. 10(a)–10(c), we can see different perspectives of the reconstructed 3D image “Blue square” from -47° to -3° which is corresponding to the LVZ. While in the RVZ, we can see different perspectives of the reconstructed 3D characters “3D” from 3° to 47°, as shown in Figs. 10(d)–10(f). The view angles of the LVZ and RVZ are about 44°, which coincide with the theoretical analysis. From -3° to 3°, however, there is crosstalk between the two 3D

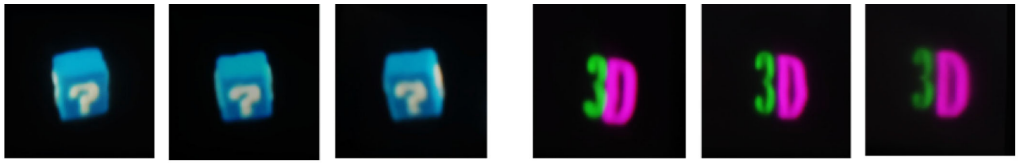

Fig. 10. 3D image reconstructed by the proposed dual-view integral imaging system, (a)–(c) 3D images in the LVZ, and (d)–(f) 3D images in the RVZ.

Fig. 11. 3D image reconstructed by the mono-view integral imaging system: (a) 3D image of 3D scene 1 and (b) 3D images of 3D scene 2.

images due to the diffused light field caused by directional diffuser screen. Figs. 11 show the reconstructed 3D images of the mono-view integral imaging system. Comparing the reconstructed 3D images in Figs. 10 and 11, they have almost the same clarity, which means both systems have the same spatial resolution. The experimental results demonstrate that the proposed dual-view integral imaging system has wide viewing angle and high spatial resolution, which is consistent with the theoretical analysis. However, the viewing angle of the dual-view integral imaging system in Ref [30] are 23° in both the LVZ and RVZ which is about half of the proposed dual-view system.

4. Conclusions

In this paper, we have proposed a dual-view integral imaging system which mainly consists of a display panel, a lens array, an electrically switchable mask and a directional diffuser screen. By synchronously switching the chessboard pattern of the switchable mask and the CEIA displayed on the display panel, a dual-view integral imaging system with wide viewing angle and high spatial resolution is achieved. The chessboard patterns on the switchable mask and the generation of the CEIA are described in detail. In this architecture, the viewing angles of the LVZ and RVZ are almost twice of the conventional dual-view integral imaging system, and the viewers in the LVZ and RVZ can see different 3D images with high spatial resolution. In the experiments, the developed experimental prototype could offer a viewing angle of 44° in each viewing zone and present 3D image with high spatial resolution.

References

[1] D. U. Kean, D. J. Montgomery, G. Bourhill, and J. Mather, "Multiple view display," U. S. Patent 7154653B2, 2010.
[2] S. Kim *et al.*, "Enabling concurrent dual views on common LCD screens," in *Proc. SIGCHI Conf. Human Factors Comput. Syst.*, 2012, pp. 2175–2184.
[3] C. P. Chen, J. H. Lee, T. H. Yoon, and J. C. Kim, "Monoview/dual-view switchable liquid crystal display," *Opt. Lett.*, vol. 34, no. 14, pp. 2222–2224, 2009.
[4] C. T. Hsieh, J. N. Shu, H. T. Chen, C. Y. Huang, C. J. Tian, and C. H. Lin, "Dual-view liquid crystal display fabricated by patterned electrodes," *Opt. Express*, vol. 20, no. 8, pp. 8641–8648, 2012.

[5] H. Choi, S.-W. Min, S. Jung, J.-H. Park, and B. Lee, "Multiple-viewing-zone integral imaging using a dynamic barrier array for three-dimensional displays," *Opt. Express*, vol. 11, no. 8, pp. 927–932, 2003.
[6] J. P. Cui, Y. Li, J. Yan, H. C. Cheng, and Q. H. Wang, "Time-multiplexed dual-view display using a blue phase liquid crystal," *J. Display. Technol.*, vol. 9, no. 2, pp. 87–90, 2013.
[7] P. A. Blanche *et al.*, "Holographic three-dimensional telepresence using large-area photorefractive polymer," *Nature*, vol. 468, no. 7320, pp. 80–83, 2010.
[8] D. Wang, C. Liu, C. Shen, Y. Xing, and Q. H. Wang, "Holographic capture and projection system of real object based on tunable zoom lens," *PhotoniX*, vol. 1, no. 1, pp. 1–15, 2020.
[9] D. Fattal, Z. Peng, T. Tran, S.Vo, M. Fiorentino, J. Brug, and R. G. Beausoleil, "A multi-directional backlight for a wide-angle, glasses-free three-dimensional display," *Nature*, vol. 495, no. 7441, pp. 348–351, 2013.
[10] W. Wan *et al.*, "Multiview holographic 3D dynamic display by combining a nano-grating patterned phase plate and LCD," *Opt. Express*, vol. 25, no. 2, pp. 1114–1122, 2017.
[11] D. E. Smalley *et al.*, "A photophoretic-trap volumetric display," *Nature*, vol. 553, no. 7689, pp. 486–490, 2018.
[12] L. Liu, Z. Pang, and D. Teng, "Super multi-view three-dimensional display technique for portable devices," *Opt. Express*, vol. 24, no. 5, pp. 4421–4430, 2016.
[13] X. Sang, X. Gao, X. Yu, S. Xing, Y. Li, and Y. Wu. "Interactive floating full-parallax digital three-dimensional light-field display based on wavefront recomposing," *Opt. Express*, vol. 26, no. 7, pp. 8883–8889, 2018.
[14] Z. Qin, P. Chou, J. Wu, C. Huang, and Y. Huang, "Resolution-enhanced light field displays by recombining subpixels across elemental images," *Opt. Lett.*, vol. 44, no. 10, pp. 2438–2441, 2019.
[15] G. Lippmann, "La photographie integrale," *C. R. Acad. Sci.*, vol. 146, pp. 446–451, 1908.
[16] M. Martinez-Corral and B. Javidi, "Fundamentals of 3D imaging and displays: a tutorial on integral imaging, light-field, and plenoptic systems," *Adv. Opt. Photon.*, vol. 10, no. 3, pp. 512–566, 2018.
[17] B. Javidi, J. Sola-Pikabea, and M. Martinez-Corral, "Recent advances in 3-D integral imaging sensing and display," *IEEE Photon. J.*, vol. 7, no. 3, Jun. 2015, Art. no. 0700907.
[18] D. Zhao, B. Su, G. Chen, and H. Liao, "360 degree viewable floating autostereoscopic display using integral photography and multiple semitransparent mirrors," *Opt. Express*, vol. 23, no. 8, pp. 9812–9823, 2015.
[19] J. Wei, S. Wang, Y. Zhao, and M. Piao, "Synthetic aperture integral imaging using edge depth maps of unstructured monocular video," *Opt. Express*, vol. 26, no. 26, pp. 34894–34908, 2018.
[20] X. Yan, J. Wen, Z. Yan, T. Zhang, and X. Jiang, "Post-calibration compensation method for integral imaging system with macrolens array," *Opt. Express*, vol. 27, no. 4, pp. 4834–4844, 2019.
[21] S. Xing *et al.*, "High-efficient computer-generated integral imaging based on the backward ray-tracing technique and optical reconstruction," *Opt. Express*, vol. 25, no. 1, pp. 330–338, 2017.
[22] Z. Wang, G. Q. Lv, Q. B. Feng, A. T. Wang, and H. Ming, "Dual-view holographic stereogram 3D display based on integral imaging," *Opt. Commun.*, vol. 454, 2020, Art. no. 124482.
[23] M. Wei, R. Fang, D. Q. Liao, and J. He, "Wide-viewing-angle dual-view one-dimensional integral imaging display," *Optik*, vol. 185, pp. 515–518, 2019.
[24] J. Jeong, C.K. Lee, K. Hong, J. Yeom, and B. Lee, "Projection-type dual-view threedimensional display system based on integral imaging," *Appl. Opt.*, vol. 53, no. 27, pp. G12–G18, 2014.
[25] M. Y. He, H.L. Zhang, H. Deng, X. W. Li, D. H. Li, and Q. H. Wang, "Dual-view-zone tabletop 3D display system based on integral imaging," *Appl. Opt.*, vol. 57, no. 4, pp. 952–958, 2018.
[26] F. Wu, H. Deng, C. G. Luo, D. H. Li, and Q. H. Wang, "Dual-view integral imaging three-dimensional display," *Appl. Opt.*, vol. 52, no. 20, pp. 4911–4914, 2013.
[27] F. Wu, Q. H. Wang, C. G. Luo, D. H. Li, and H. Deng, "Dual-view integral imaging 3D display using polarizer parallax barriers," *Appl. Opt.*, vol. 53, no. 10, pp. 2037–2039, 2014.
[28] Q. H. Wang, C. C. Ji, L. Li, and H. Deng, "Dual-view integral imaging 3D display by using orthogonal polarizer array and polarization switcher," *Opt. Express*, vol. 24, no. 1, pp. 9–16, 2016.
[29] F. Wu, G. J. Lv, H. Deng, B. C. Zhao, and Q. H. Wang, "Dual-view integral imaging three-dimensional display using polarized glasses," *Appl. Opt.*, vol. 57, no. 6, pp. 1447–1449, 2018.
[30] Y. Xing, Q. H. Wang, L. Luo, H. Ren, and H. Deng, "High-Performance Dual-View 3-D Display System Based on Integral Imaging," *IEEE Photon. J.*, vol. 11, no. 1, 2019, Art. no. 7000212.
[31] B. Y. Liu *et al.*, "Multi-rays computational floating light-field display based on holographic functional screen," *Optik*, vol. 172, pp. 406–411, 2018.
[32] H. Deng, Q. H. Wang, L. Li, and D. H. Li, "An integral-imaging three-dimensional display with wide viewing angle," *J. Soc. Inf. Display*, vol. 19, no. 10, pp. 679–684, 2011.
[33] S. W. Min, J. Kim, and B. Lee, "New characteristic equation of three-dimensional integral imaging system and its applications," *Japanese J. Appl. Phys.*, vol. 44, no. 2, pp. L71–L74, 2005.